Reactivity of Chars and Carbons: New Insights through Molecular Modeling

S. K. Bhatia
Cooperative Research Centre for Black Coal Utilisation, Dept. of Chemical Engineering,
The Univ. of Queensland, Brisbane, Queensland 4072, Australia

A new model proposed for the gasification of chars and carbons incorporates features of the turbostratic nanoscale structure that exists in such materials. The model also considers the effect of initial surface chemistry and different reactivities perpendicular to the edges and to the faces of the underlying crystallite planes comprising the turbostratic structure. It may be more realistic than earlier models based on pore or grain structure idealizations when the carbon contains large amounts of crystallite matter. Shrinkage of the carbon particles in the chemically controlled regime is also possible due to the random complete gasification of crystallitic planes. This mechanism can explain observations in the literature of particle size reduction. Based on the model predictions, both initial surface chemistry and the number of stacked planes in the crystallites strongly influence the reactivity and particle shrinkage. Its test results agree well with literature data on the air-oxidation of Spherocarb and show that it accurately predicts the variation of particle size with conversion. Model parameters are determined entirely from rate measurements.

Introduction

The reactivity of chars and various carbonaceous materials to oxygen, carbon dioxide, and steam has long been a subject of investigation. The understanding of the factors influencing reactivity, apart from being relevant to gasification processes and improved operation of gasifiers and combustion systems, is important to several newer applications. These applications include the activation of carbonaceous materials to produce various microporous adsorbents and the integrity of structural carbons and composites that are often required to withstand adverse environments without failure.

Several models have been proposed in the literature for predicting the effect of process variables on the reaction rates of chars and carbons in various environments. The simplest model assumes that reaction occurs on the external surface of shrinking particles (Szekely et al., 1976), thereby ignoring internal reaction. Internal reaction is, however, generally the dominant contributor to the overall rate, even in the presence of a strong diffusional resistance whereby reaction occurs predominantly in a narrow zone near the shrinking external boundary (Bhatia, 1991a,b). Models considering internal reaction include the volume and grain reaction models (Szekely et al., 1976), and those that focus on the pore structure (Petersen, 1957; Bhatia and Perlmutter, 1980; Gavalas, 1980). The volume and grain reaction models have the deficiency that they cannot predict a rate maximum with increase in conversion in the chemically controlled regime, as is commonly observed (Su and Perlmutter, 1985; Chi and Perlmutter, 1989). This feature can be predicted by the random pore models (Petersen, 1957; Bhatia and Perlmutter, 1980; Gavalas, 1980), which consider the competing mechanisms of pore growth and overlap. The effect of these mechanisms is characterized by a unique model-specific structural parameter in each case. However, the values of the structural parameter determined from characterization studies and from correlation of rate data are often divergent (Miura et al., 1990), or sometimes unrealistic (Kasaoka et al., 1985). These results suggest the need for further investigation of the factors influencing reactivity and improved model development. Other pore structure-based models exist that provide greater flexibility at the expense of additional parameters. In most cases, however, the difficulty of independently measuring such parameters and the added fitting complexity has resulted in these models receiving much less attention. Many of these models, as well as other models which apply to restricted pore

structures, have therefore found limited usefulness and are discussed elsewhere (Bhatia and Gupta, 1992).

In the literature a significant body of evidence has developed that the structure of chars and carbons has a substantial component comprising stacked planar aromatic sheets organized in the form of small crystallites (Ben-Aim, 1987; Davis et al., 1994; Babu and Seehra, 1996). This latter structure is often termed "turbostratic," as the sheets do not necessarily have the same relative organization and spacing as in graphite. Although this has also been reported much earlier (Biscoe and Warren, 1942; Franklin, 1951), most models have developed along the different lines discussed above. These studies have revealed that the crystallites comprise 3–7 stacked sheets of 2–4 nm diameter, with an interplanar spacing of about 0.34 nm. Clearly the reaction models discussed above do not incorporate such crystalline-like structures, and therefore cannot consider the associated anisotropy in reactivities. Indeed, much experimental evidence exists that the edge sites on graphite sheets or planes have a higher reactivity than the internal ones (Horton, 1961; Thomas and Jones, 1964; Hennig, 1965; Ben-Aim, 1987). This has recently also been theoretically confirmed by Kyotani et al. (1996) for single aromatic sheets using molecular orbital theory. In the computations of Kyotani et al., the edge sites were found to have a reactivity about three times that of the internal reaction sites. This factor is a reasonable average for the various kinds of edge sites, comprising armchair, zig-zag, and D-type sites (Ben-Aim, 1987; Kyotani et al., 1993), and is consistent with the finding of Horton (1961) that the thickness of graphite plates obtained by cleavage decreased four times as slowly as their diameter during oxidation.

Apart from their lack of conformity with the above experimental observations of the structure and reactivity of carbons, the existing models discussed earlier are currently also unable to predict several important and unusual features reported for char gasification. These features include observations of gasification-induced particle shrinkage, even in the chemically controlled regime. This effect has been reported for a variety of carbonaceous materials, including coal chars and activated carbon (Hurt et al., 1988; Wong et al., 1995), form coke (Easler et al., 1990), and soot (Ishiguro et al., 1991), and found (Hurt et al., 1988, 1993) to occur homogeneously at all scales of observation from the microscopic to macroscopic. Among the proposed explanations for this intriguing phenomenon are atomic rearrangements at the crystallite level (Hurt et al., 1988, 1993; Easler et al., 1990), and stripping and disintegration of surface carbon layers (Ishiguro et al., 1991), though the latter is inconsistent with the observation of shrinkage at the microscale. However, the concept of atomic rearrangements also seems unlikely to apply to the low temperatures ($< 1{,}000$ K) at which shrinkage has been reported by various investigators. This is supported by the results of Senneca et al. (1997) showing the time scale of annealing to be several orders of magnitude higher than that for reaction in oxygen below 1,000 K. A more detailed analysis of the findings is required to establish the mechanism.

Another important feature reported for char gasification that is currently not considered in the various models is the role of surface chemistry. From their study of CO_2 gasification of coal chars, Kasaoka et al. (1985) concluded that the rate was more closely controlled by the chemical properties of the char surface than by its composition and pore structure. In other studies Yang and Duan (1985) reported the inhibition of the $C–CO_2$ reaction by chemisorbed hydrogen, while Menendez et al. (1996) observed this for the $C–O_2$ reaction as well. Furthermore, based on an analysis of published results Ben-Aim (1987) noted the blocking effect of surface oxides and inhibition of reactivity. Among these results is the important finding of Letort (1960) that the rate of oxidation of a previously oxidized graphite surface is greater than that of the unoxidized one, and that of Bonnetain and Hoynant (1965) that after oxidation and degassing near 1,173 K the rate of oxidation increased and tended to a limiting value. The latter would be explained by an estimate of Laine et al. (1961) that 95% of the surface oxides are removed by degassing at 1,173 K. All of these results have been confirmed and lucidly explained in the recent work of Menendez et al. (1996), who conclude that stable surface C–H bonds formed on high temperature exposure to H_2 retard oxidation, and that degassing at high temperatures removes surface oxides and liberates very reactive unsaturated carbon atoms. None of the existing models considers such effects, so the role of surface chemistry remains to be addressed. It may be noted, however, that the recent modification of the random pore model (Bhatia and Vartak, 1996), recognizing discreteness of the solid, does provide a framework in which surface chemistry and the different reactivities of the initial and reacted surfaces can be incorporated. This is being investigated in our laboratory and will be reported in a forthcoming publication.

Although it may be possible to address the problems of shrinkage and surface chemistry within the framework of existing grain or pore models, the evidence regarding turbostratic structure does suggest the need to develop a new class of models more consistent with this geometry. To this end we propose a new reactivity model based on the concept of the char or carbon being composed of small crystallites having stacked planes of aromatic sheets, based on the evidence discussed earlier. The model incorporates the differences in both the reactivities of edge and internal sites on the planes and the initial surface chemistry by considering the effect of functional groups on the initial edges of the planes. Most interestingly, the model can also accurately predict the observed shrinkage in the chemical control regime without recourse to fitting parameters. It may be noted that the model of Kantorovich and Bar-Ziv (1994) predicts shrinkage. However, their model considers a skeleton of carbon microrods and macrorods that does not well represent the turbostratic structure. In addition, it utilizes somewhat complex mechanisms of rod coalescence and joint breakage and rejoining at rod intersections, which are difficult to experimentally confirm. Although crystallite reaction models exist in the literature (Wolff, 1959; Miura and Hashimoto, 1984), these models involved the unphysical assumption of instantaneous gasification of a complete plane and did not consider the subsequently recognized issue of shrinkage. More interesting perhaps are the recent attempts at studying the gasification of single planes (Kyotani et al., 1993, 1996) that, while not addressing the issues of surface chemistry and shrinkage, provide useful insights into the reaction behavior and mechanism. The present work takes the next major step in moving from the level of a single plane to that of an agglomerate of

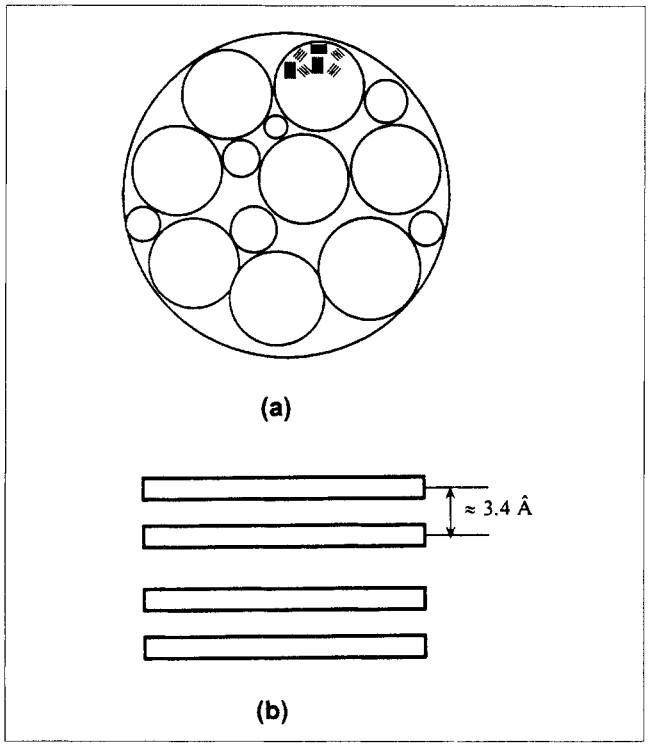

Figure 1. Idealized solid structure.

(a) Particle comprising spherical grains, with the grains containing aggregated crystallites; (b) the planes in a crystallite.

crystallites, albeit with some simplifying assumptions. Further, our approach is analytical, in contrast to the simulative approaches of Kyotani et al. (1993, 1996).

While the present article addresses the structural concerns, it may be noted that reports also exist (Lizzio et al., 1990; Chen et al., 1993; Moulijn and Kapteijn, 1995) that the accumulation of surface complexes can play a significant role in the reaction dynamics. While such effects may indeed occur, in a large variety of situations it may be anticipated that apparently pseudo-steady state conditions on the surface will be established (Bhatia, 1987a). Under these conditions structural effects will dominate. This is indeed supported by the observations of surface area and rate maximima at about the same conversion in several cases (Su and Perlmutter, 1985; Chi and Perlmutter, 1989). Consequently, in the present work we have focused on the structural issues, with the addition of chemisorption and surface dynamics to be considered subsequently.

Mathematical Model

Physical basis and assumptions

The approach proposed here utilizes the following central assumptions:

1. The char or carbon particles comprise an aggregate of spherical grains, which themselves further comprise an agglomerate of crystallites, as depicted in Figure 1a. The applicability of the grain structure model is supported by the particle-size independence of intraparticle transport rates (Bhatia, 1987b) for sufficiently small particles.

2. Each crystallite consists of a stack of H planes spaced 0.34 nm apart, as shown in Figure 1b.

3. Each plane comprises an aromatic sheet with functional groups at the edge sites as shown in Figure 2a below. Reaction at an edge site opens up further unsaturated valences at neighboring edge sites, making them more reactive. Thus, the rate of reaction along the perimeter is anticipated to be much larger than that in the radial direction. As a simplification of this picture we idealize each plane as comprising m circular rings of carbon atoms. Reaction of the edge atoms on a plane is then assumed to occur layerwise, with the carbon atoms in the outermost layer (ring) reacting together, as depicted in Figure 2b below. For the initial outermost layer, with functional groups attached, the rate constant is k_1, while for the subsequent layers the rate constant is k_2. For the subsequent layers the exposed carbon atoms are unsaturated and more reactive, so that $k_2 > k_1$. These constants are assumed to hold for all edge sites regardless of type (zig-zag, D-type, or armchair). In the absence of detailed characterization of the ini-

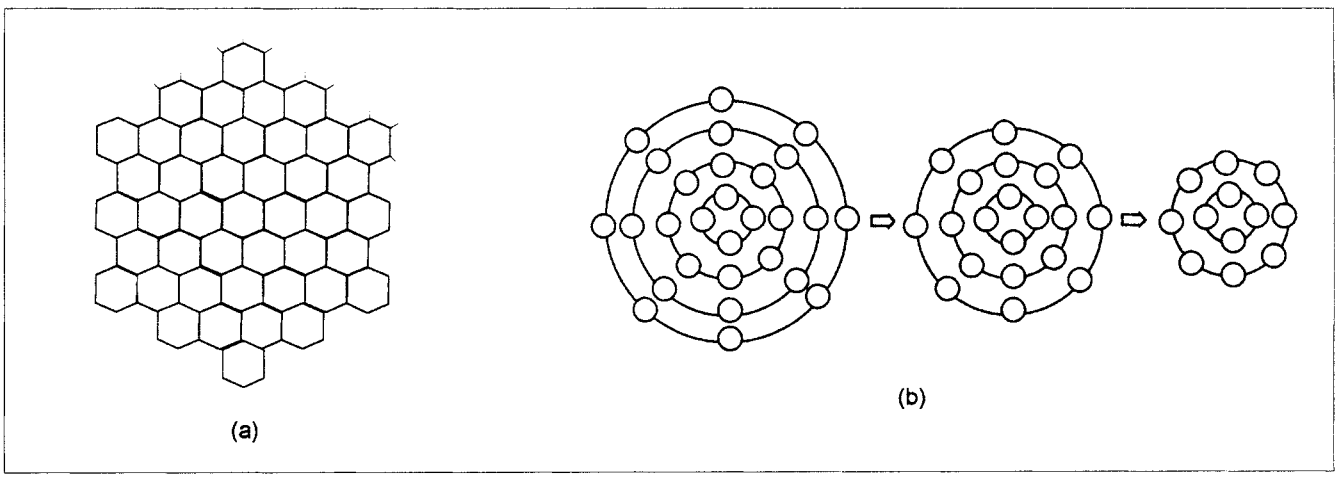

Figure 2. Crystallite plane.

(a) Actual aromatic structure with functional groups at the edge; (b) idealized configuration comprising rings of carbon atoms, with the atoms on a ring gasified simultaneously.

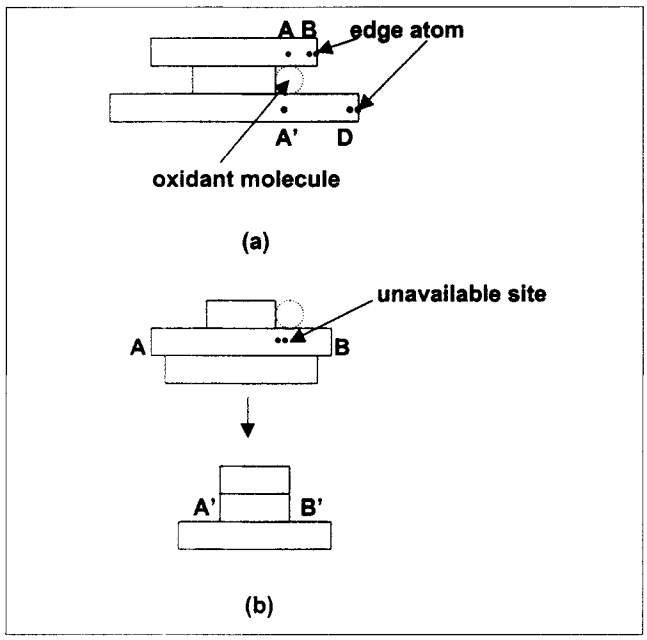

Figure 3. Reaction of crystallite planes.

(a) Edge and internal sites; (b) gasification on planar surface.

tial site distribution and the aromatic structures permitting prediction of the distribution of new sites created, this simplifying assumption is justified. In the future when more detailed knowledge is available the assumption may be relaxed.

4. It is assumed that the oxidant or gasifying agent cannot penetrate the interplanar space between neighboring planes. For a plane sandwiched between larger planes, however, the edge sites are considered exposed to the gas and therefore available for reaction. In this case the exposed internal carbon atoms on the upper and lower planes of the sandwich in the regions AB and A'D are also available for reaction from within the sandwich as depicted in Figure 3a.

5. The two bounding planes of the crystallite have functional groups attached on their planar surfaces. A fresh planar surface within the crystallite, as shown (AB or A'D) in Figure 3a, is assumed to have a reaction rate constant k_3 for reaction from each exposed side in the sandwich. The two externally exposed initial bounding planar surfaces of the crystallite, having attached functional groups, are assumed to have a reaction rate constant k_4. Furthermore, we assume that the functional groups retard the reaction at the internal sites to the same extent as at the edge sites, so that

$$k_4 = \frac{k_1}{k_2} k_3 = \frac{k_3}{A} \tag{1}$$

where $A = k_2/k_1$. It is this factor A that reflects the role of the initial surface chemistry. Further refinement, such as a distribution of A values (or of an associated Arrhenius activation energy difference between initial and new sites), is also possible but not considered in the present work. Such a distribution would reflect the surface heterogeneity long-recognized in the analysis and interpretation of adsorption isotherms (Rudzinski and Everett, 1992) and is therefore an important future direction for the new approach.

6. The ratio of the reactivity of new edge sites to new internal sites is e, with the value $e = 3$ being a good representation of the results of Kyotani et al. (1996). Thus,

$$\frac{k_2}{k_3} = \frac{k_1}{k_4} = e \tag{2}$$

7. When an exposed planar surface reacts, the entire exposed part is instantaneously gasified. Thus, in one step the plane reacts to a size equalling the smaller of the two neighboring planes, as depicted by $AB \rightarrow A'B'$ in Figure 3b, regardless of which side the oxidant attack occurs from. This assumption is realistic because if an internal exposed site reacts, a hole with surrounding unsaturated carbons is created. These unsaturated atoms will be extremely reactive, leading to rapid gasification of the entire exposed surface, regardless of the side in which the initial hole-forming attack occurred. This point of view is supported by the recent simulations of Kyotani et al. (1996).

8. Due to the random nature of the layerwise reaction, a plane can be completely gasified even though the neighboring planes are larger and still reacting. In such a case shrinkage of the crystallite occurs with the neighboring planes coming together to close the gap created. This shrinkage is predominantly a result of the attractive van der Waals forces between the planes, and is assumed to be transmitted homogeneously at all length scales in the particle, following the observations of Hurt et al. (1988).

9. The agglomerate in a grain is composed of randomly overlapping crystallites at all times during gasification. This simulates defective crystallites fused and cross-linked with others, and having angular boundaries, as is commonly believed to occur. The properties of such randomly overlapping entities have been dealt with in the context of gasification in earlier work (Bhatia and Perlmutter, 1980; Gavalas, 1980; Adschiri et al., 1987), and are used in the present analysis.

Structural characterization

The surface area of porous solids forms one of their key characteristic variables, usually measured by adsorption. Here we develop a relation between the structural parameters H and m, and the initial surface area. To this end we first characterize the initial crystallites by estimating the relation between diameter and number of rings. Assuming neighboring carbon atoms to be close-packed on a plane, one obtains

$$h = \frac{\sqrt{3}}{2} d \tag{3}$$

where h is the radial distance between successive rings, and d the center-to-center distance between carbon atoms. This yields the number of sites in the nth ring or layer as

$$N_n \simeq \frac{2\pi h(m - n + 1)}{d} = \sqrt{3}\,\pi(m - n + 1) \tag{4}$$

in which N_n represents number of sites in the nth layer and $n = 1$ corresponds to the outermost ring. In this notation $n =$

m corresponds to the innermost layer (ring), circumscribing a single aromatic ring. The quantity N_n is always taken as the smallest integer larger than the value evaluated from Eq. 4. The total number of carbon atoms in a plane is then obtained as

$$N_t(m) = \sum_{n=1}^{m} N_n = \frac{\sqrt{3}}{2}\pi m(m+1) \tag{5}$$

and the volume of a crystallite as

$$V_c = \pi m^2 h^2 \delta (H-1) \tag{6}$$

in which δ is the interplanar separation (measured between centers of carbon atoms), here taken as 0.34 nm. This yields the crystallite density

$$\rho_t = \frac{N_t H M_c}{V_c} = \frac{\sqrt{3}\, m(m+1) H M_c}{2m^2 h^2 \delta (H-1) N_a} \tag{7}$$

We now assume that for large crystallites the density ρ_t is the same as that of graphite, having the value 2,260 kg/m^3, and yields $h = 0.15$ nm. The measured initial specific surface area of the crystallite is evaluated as

$$S_{eg} = \frac{2\pi (r_2 H\delta + r_1^2) N_a}{M_c N_t H} \tag{8}$$

in which

$$r_1 = mh \tag{9}$$

is the initial crystallite radius, and

$$r_2 = r_1 + \sigma_{fs} \tag{10}$$

is the radius of the surface on which the centers of the first layer of adsorbate molecules lie. Here σ_{fs} is the distance between the centers of the carbon atoms and the adsorbate molecules with 0.35 nm taken as a typical value. This corresponds well with the size parameter (Seaton et al., 1989) of the Lennard Jones potential for the nitrogen carbon interaction. Substituting values of h, δ, σ_{fs} and N_a, and combining Eqs. 5, 8–10 we obtain

$$S_{eg} = \frac{5{,}912[H(m+2.33) + 0.4412\ \text{m}^2]}{mH(m+1)}, \quad \text{m}^2/\text{g} \tag{11}$$

As indicated in assumption (9), the crystallites are considered randomly overlapping so that, following the earlier analyses (Bhatia and Perlmutter, 1980; Gavalas, 1980) for randomly overlapping entities,

$$V_{es} = \ln(1/\epsilon_\mu) \tag{12}$$

where V_{es} is the volume of nonoverlapped crystallites per unit grain volume, and ϵ_μ is the grain microporosity. Assuming that the crystallite solid-phase density does not change on overlapping, we now obtain the resulting initial specific surface area as

$$S_g = \frac{S_{eg}\, \rho_t V_{es} \epsilon_{\mu 0}}{\rho_t (1-\epsilon_{\mu 0})} = \frac{5{,}912[H(m+2.33) + 0.4412\ \text{m}^2]\epsilon_{\mu 0} \ln(1/\epsilon_{\mu 0})}{m(m+1)H(1-\epsilon_{\mu 0})}, \quad \text{m}^2/\text{g} \tag{13}$$

This completes the characterization of the initial crystallites. As is common for most existing structural models, such as the random pore model, three parameters are needed to characterize internal structure of the grains. These could be m, H, and $\epsilon_{\mu 0}$ with S_g being a derived parameter. In case of the pore structure models the parameters are usually the mean pore size, dispersion parameter of the micropore size distribution and the grain microporosity.

Analysis of crystallite evolution

As assumed in the present work, all the crystallite planes initially have the same size m (the number of layers or rings of carbon atoms). As gasification is initiated at the exposed edges and the upper and lower basal planes [with these planes having a lower reactivity, as discussed in assumption (5)], the sizes of the different planes will not remain the same. To describe the evolution of the different planes we define a probability $P_{in}(t)$ that the edge of the ith plane is at position n at time t. The planes are indexed sequentially with the top plane having the index $i = 1$ and the bottom plane $i = H$. As indicated earlier the index $n = 1$ at the initial edge of the planes (m layers away from the center) and increases to m at the innermost ring. Figure 4 illustrates this numbering scheme. A master equation may now be developed for the evolution of $P_{in}(t)$, as follows.

$$\frac{dP_{in}}{dt} = -k_{in}P_{in} + k_{i(n-1)}P_{i(n-1)} - T_{in} - B_{in} + \sum_{k=1}^{n-2} k_{ik}^{(1)} P_{ik} R_{ink}, \quad i = 1, 2, \ldots, H;\ n = 1, 2, \ldots, m \tag{14}$$

Here the first term in the righthand side represents the rate of transition of the edge of the ith plane from n to $(n+1)$, while the second term is the rate of transition from $(n-1)$ to

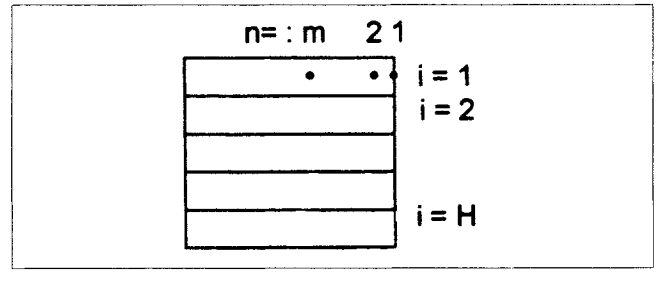

Figure 4. Indexing scheme for crystallite planes and carbon rings on a plane.

The index m takes on the values of 1, 2, ..., m, starting from the initially outermost ring of carbon atoms.

n. The rate constant k_{in} has the value

$$k_{in} = k_2/A, \quad n = 1$$
$$= k_2, \quad n > 1 \tag{15}$$

following assumption (3) and (5). The third term in the righthand side of Eq. 14, T_{in}, represents the evolution rate of P_{in} due to gasification of the ith plane at its exposed surface on the upper side, and the fourth term B_{in} similarly represents the rate due to gasification at its exposed surface on the lower side. Finally, the last term in the righthand side of Eq. 14 represents the rate of increase of P_{in} due to gasification of the ith plane on its upper and lower exposed surfaces. Since gasification of the entire exposed surface is instantaneous, following assumption (7), transition of the edge of the ith plane into location n could in principle occur from any location having an index less than n when surface reaction occurs. However, since the distance parameter $\sigma_{fs} > 2h$, we assume that the innermost exposed layer is unavailable for reaction, as depicted in Figure 3. The term R_{ink} in Eq. 14 then represents the probability of transition of the edge of the ith plane from location k to location n, due to reaction on the upper and lower surfaces, and $k_{ik}^{(1)}$ the corresponding rate constant (to be specified later).

It is now necessary to relate the terms T_{in}, B_{in} and R_{ink} in the righthand side of Eq. 14 to P_{in}. For the term T_{in} it is recognized that the plane above (having index ℓ) covering part of the ith plane may be any of the upper planes between 1 and $(i+1)$, both inclusive, with the planes between this and the ith plane having been completely gasified. The absence of these completely gasified in-between planes leads to shrinkage and closure of the gap between the ith and ℓth planes, following assumption (8). Furthermore, this latter plane may have any size index between $(n+2)$ and m for a portion of the upper surface of the ith plane to be available for reaction (Figure 6). Accordingly, we may write the rate of change of P_{in} due to gasification on the upper surface as

$$T_{in} = k_{in}^{(1)} P_{in} \left[\left(\sum_{j=n+2}^{m} \sum_{\ell=1}^{i-1} P_{\ell j} \prod_{s=\ell+1}^{i-1} (q_s) \right) + \prod_{s=1}^{i-1} (q_s) \sum_{\ell=1}^{m-1} \delta_{\ell n} \right] \tag{16}$$

where $\delta_{\ell m}$ is the Kronekar delta function. Here q_s represents the probability that the sth plane has been completely gasified and is absent at time t, so that

$$q_s = 1 - \sum_{n=1}^{m} P_{sn} \tag{17}$$

The second term in the square brackets in the righthand side of Eq. 16 represents the probability that all planes above the ith have been gasified away, so that the ith plane is now the top plane. A plane having only a single ring ($n = m$) is considered to have only an edge and no planar surface. Furthermore, in Eq. 16, following assumptions (5) and (6),

$$k_{in}^{(1)} = k_3 = k_2/e, \quad i > 1; \; n = 1, 2, \ldots, m$$
$$= k_4 = k_3/A = k_2/(Ae), \quad i = 1; \; n = 1, 2, \ldots, m \tag{18}$$

since the top of the plane $i = 1$ is the initial less reactive surface. This equation also specifies the rate constant in the last term in the righthand side of Eq. 14. Similarly, for the reaction on the lower side of plane i,

$$B_{in} = k_{in}^{(2)} P_{in} \left[\left(\sum_{j=n+2}^{m} \sum_{\ell=i+1}^{H} P_{\ell j} \prod_{s=i+1}^{\ell-1} (q_s) \right) + \prod_{s=i+1}^{H} (q_s) \sum_{\ell=1}^{m-1} \delta_{\ell n} \right] \tag{19}$$

where

$$k_{in}^{(2)} = k_2/e, \quad i < H; \; n = 1, 2, \ldots, m$$
$$= k_2/Ae, \quad i = H; \; n = 1, 2, \ldots, m \tag{20}$$

To determine the transition probability R_{ink} for plane i to instantaneously gasify from size k to size n, it is again necessary to consider the processes on the upper and lower surfaces of the ith plane. For these we identify four possibilities.

- The plane above the ith plane has edge location between $(k+2)$ and $(n-1)$, and the plane below has edge location n. In this case, even if attack occurs from above the ith plane will gasify to size n, following assumption (7). As before, recognizing that the plane immediately above can have any index ℓ lying between 1 and $(i-1)$, and the plane below any index between $(i+1)$ and H, with the in-between planes having been gasified away, the probability for this process may be expressed as

$$R_{ink}^{(1)} = \left[\sum_{j=k+2}^{n-1} \sum_{\ell=1}^{i-1} P_{\ell j} \prod_{s=\ell+1}^{i-1} (q_s) \right] \cdot \left[\sum_{\ell=i+1}^{H} P_{\ell n} \prod_{s=i+1}^{\ell-1} (q_s) \right]$$
$$i = 1, 2, \ldots, H; \; n = 1, 2, \ldots, m; \; k = 1, 2, \ldots, (n-2) \tag{21}$$

The first set of square brackets in the righthand side of the above equation contains the contribution to the probability from the plane above, and the second set the contribution from the plane below (having fixed edge location n to which plane i gasifies). Furthermore, for the upper exposed surface to be available, at least two layers must be exposed (see Figure 3). Thus, the plane above has a size index of at least $(k+2)$.

- The plane above has edge location at n, and the plane below has any random edge location between 1 and n (both inclusive). In a manner similar to that above we obtain

$$R_{ink}^{(2)} = \left[\sum_{\ell=1}^{i-1} P_{\ell n} \prod_{s=\ell+1}^{i-1} (q_s) \right] \left[\sum_{j=1}^{n} \sum_{\ell=i+1}^{H} P_{\ell j} \prod_{s=i-1}^{\ell-1} (q_s) \right] \tag{22}$$

with the domain of i, n, and k being the same as in Eq. 21.

• The plane above has edge location at n, and the plane below has edge location between $(k+2)$ and $(n-1)$. Again, recognizing that the initial in-between planes on each side may have been completely gasified, we obtain, as in Eq. 21

$$R_{\text{ink}}^{(3)} = \left[\sum_{j=k+2}^{n-1} \sum_{\ell=i+1}^{H} P_{\ell j} \prod_{s=i+1}^{\ell-1} (q_s)\right]\left[\sum_{\ell=1}^{i-1} P_{\ell n} \prod_{s=\ell+1}^{i-1} (q_s)\right] \tag{23}$$

with the indices i, n, and k having the same domain as in Eq. 21.

• The plane below has edge location at n, and the plane above has edge location between 1 and n. In a manner similar to the section with Eq. 22 above, we obtain the probability for this mechanism as

$$R_{\text{ink}}^{(4)} = \left[\sum_{\ell=i+1}^{H} P_{\ell n} \prod_{s=i+1}^{\ell-1} (q_s)\right]\left[\sum_{j=1}^{n} \sum_{\ell=1}^{i-1} P_{\ell j} \prod_{s=\ell+1}^{i-1} (q_s)\right] \tag{24}$$

with the indices i, n, and k having the same domain as in Eq. 21.

The four contributions listed above may now be combined in the form

$$R_{\text{ink}} = R_{\text{ink}}^{(1)} + R_{\text{ink}}^{(2)} + R_{\text{ink}}^{(3)} + R_{\text{ink}}^{(4)} \tag{25}$$

to yield the overall transition probability required for use in Eq. 14. Equations 14–25 now completely specify the evolution of the crystallites in their nonoverlapped forms, given the initial conditions

$$P_{\text{in}}^{0}(0) = P_{\text{in}}^{0} = \delta_{n1}, \quad i = 1, 2, \ldots, H; \; n = 1, 2, \ldots, m \tag{26}$$

which assert that each sheet (or plane) has initial edge location at $n = 1$ (has m rings of carbon atoms).

Evolution of structure and conversion

Once the probability distribution $P_{\text{in}}(t)$ for the edge locations of the crystallite planes is determined through Eqs. 14–26, it is possible to estimate the evolution of the pore structure and the conversion. To accomplish this we first evaluate the shrinkage of the pellet due to complete gasification of planes. Following the observations of Hurt et al. (1988), and assumption (8), the shrinkage is homogeneously transmitted at all scales. We may therefore evaluate the fractional volume loss, or shrinkage, at any time as

$$Q(t) = \frac{1}{H} \sum_{i=1}^{H} q_i(t) \tag{27}$$

which leads to

$$\left(\frac{R(t)}{R_0}\right)^3 = 1 - Q(t) = \frac{1}{H} \sum_{i=1}^{H} \sum_{j=1}^{m} P_{ij}(t) \tag{28}$$

The porosity of the grains at any time may be evaluated by means of Eq. 12, which considers the crystallites as randomly overlapping [see assumption (9)]. To relate υ_{es} to the probability distribution, we consider the radius of any plane having edge location n as

$$r = h(m - n + 1) \tag{29}$$

leading to

$$\upsilon_{\text{es}}(t) = \pi h^2 \delta N_{\upsilon} \sum_{i=1}^{H} \sum_{n=1}^{m} (m - n + 1)^2 P_{\text{in}}(t) \tag{30}$$

where N_{υ} represents the number of crystallites per unit volume. This quantity must vary with time according to

$$N_{\upsilon}(t) = \frac{N_{\upsilon}^{0}}{[1 - Q(t)]}, \tag{31}$$

which accounts for the homogeneous shrinkage. Furthermore, following Eq. 30, the initial value of V_{es} is given as

$$V_{\text{esO}} = \pi h^2 \delta N_{\upsilon}^{0} \sum_{i=1}^{H} \sum_{n=1}^{m} (m - n + 1)^2 P_{\text{in}}^{0} \tag{32}$$

Equations 12 and 30–32 now provide

$$\epsilon_{\mu}(t) = \epsilon_{\mu 0}^{\sum_{i=1}^{H} \sum_{n=1}^{m} (m-n+1)^2 P_{\text{in}}/(1-Q)} \Big/ \sum_{i=1}^{H} \sum_{n=1}^{m} (m-n+1)^2 P_{\text{in}}^{0} \tag{33}$$

In the case of initially uniform crystallites, as considered here, P_{in}^{0} follows Eq. 26 and

$$\epsilon_{\mu}(t) = \epsilon_{\mu 0}^{\sum_{i=1}^{H} \sum_{n=1}^{m} (m-n+1)^2 P_{\text{in}}/(1-Q) m^2 H} \tag{34}$$

To estimate the conversion at any time we first consider the fractional loss in volume of the solid phase, given by

$$f = 1 - \frac{(1 - Q)(1 - \epsilon_{\mu})}{(1 - \epsilon_{\mu 0})} \tag{35}$$

Conventionally, this ratio is considered equal to the conversion based on the assumption that the solid phase density is constant. This assumption can be strictly valid only for infinitely large crystallites. In the present case, since the crystallites associated with the turbostratic structure generally comprise only a few (3–7) planes, each of which has 5–10 layers (rings) of carbons, such an assumption is likely to be erroneous. To correct for this we consider the number of carbon atoms in a crystallite, and obtain for the density

$$\rho_t \alpha \frac{\sum_{i=1}^{H} \sum_{n=1}^{m} N_t(n) P_{\text{in}}}{\sum_{i=1}^{H} \sum_{n=1}^{m} (m - n + 1)^2 P_{\text{in}}} \tag{36}$$

in which the numerator represents the number of carbon atoms in a crystallite, and the denominator is proportional to its volume. Combining Eqs. 35 and 36, we obtain the expression for the conversion as

$$x = 1 - \frac{\rho_t(1-f)}{\rho_{to}} = 1 - \frac{(1-Q)(1-\epsilon_\mu)\left[\sum_{i=1}^{H}\sum_{n=1}^{m} N_t(n)P_{in}\right]\left[\sum_{i=1}^{H}\sum_{n=1}^{m}(m-n+1)P_{in}^0\right]}{(1-\epsilon_{\mu 0})\left[\sum_{i=1}^{H}\sum_{n=1}^{m}(m-n+1)^2 P_{in}\right]\left[\sum_{i=1}^{H}\sum_{n=1}^{m} N_t(n)P_{in}^0\right]} \quad (37)$$

Equations 28, 33 and 37 provide the necessary relations for evaluating the conversion, for any instantaneous probability distribution $P_{in}(t)$. In addition to the shrinkage factor and the grain porosity, often one is also interested in the surface area and the pore size distribution. Although the current model can be used to evaluate these, they have not been investigated in this pilot study, and will be examined in our future work in the area.

Results and Discussion

The model described above provides a versatile framework for incorporating the effects of surface chemistry and gasification-induced shrinkage on the reactivity, while representing key features of the turbostratic structure inherent to most chars and carbons. The model as developed is locally applicable at any point in a particle, with the rate constant k_1–k_4 depending on the local gaseous reactant concentration. In the presence of diffusional and heat-transfer resistances suitable transport models, as well as models for the temperature- and concentration-dependence of the rate constants, can be combined with the present local reactivity model to predict the evolution of the system. In the isothermal case with reaction control and negligible effect of chemisorption dynamics, however, the model can be used globally with fixed rate constants. Since the extension to include heat and mass transport effects is well established, we confine our attention to the isothermal chemical control case, which is sufficient to explore the features of the new model. The model has the six parameters H, m, ϵ_μ, k_2, A and e, of which the first three are structural and the next three are kinetics-related. Computations were initially performed to investigate the effect of these parameters on the process behavior in the isothermal, chemically controlled regime. For solving the system of differential equations (Eqs. 14–26) an explicit fourth-order Runge-Kutta technique was used. A FORTRAN program implemented on a Pentium-233 microcomputer required only about 30 s of CPU time for execution in the case of $H = 4$, $m = 8$. For larger crystallites this time increased.

Crystallite evolution

Initially the evolution of the crystallites was examined for the case of $H = 7$, $m = 10$, $\epsilon_\mu = 0.2$, $A = 2$ and $e = 3$, with time rendered dimensionless using the substitution $\tau = k_2 t$. Figure 5 depicts the probability distribution of the different planes at 50% conversion ($x = 0.5$). For the top two ($i = 1, 2$) and bottom two ($i = 6, 7$) planes the highest probability is for complete gasification ($n = 11$), although for the nongasified planes with these indices the most probable size corresponds to about $n = 5$. The inner planes of the crystallite, however, are much less likely to be gasified away; the probability of

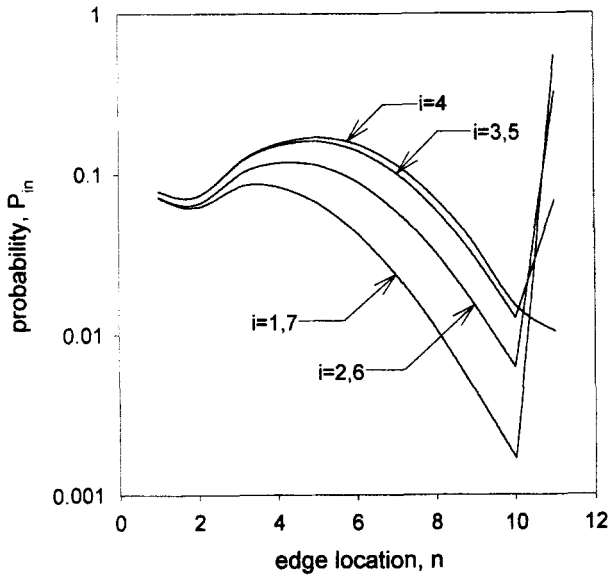

Figure 5. Probability distribution for the edge location of different crystallite planes at 50% conversion.

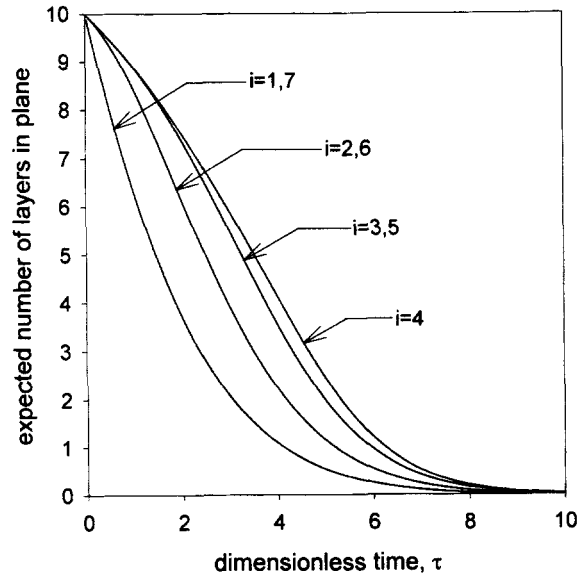

Figure 6. Temporal variation of expected number of carbon rings (or layers) in the different planes for $A = 2$.

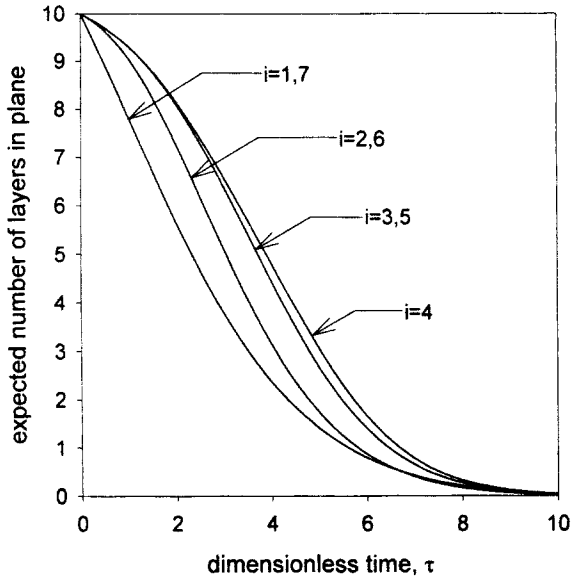

Figure 7. Temporal variation of expected number of carbon rings (or layers) in the different planes for $A = 3$.

this is less than 0.1 for $i = 3$, 5 and about 0.01 for $i = 4$ (the middle plane). The outer planes may therefore be expected to react at a higher rate than the inner ones, with the innermost reacting the slowest. These reaction rates are clearly due to the larger exposed surface of the outer planes. Figure 6 depicts the temporal variation of expected number of carbon layers (rings) in the various planes, calculated using

$$N_{\mathrm{Li}}(t) = \sum_{n=1}^{m} (m - n + 1) P_{\mathrm{in}}(t) \tag{38}$$

and confirming the higher reactivity of the outer layers. That this larger reactivity of the outer planes is related to the larger exposed surface is evident from the initial slopes of the curves in Figure 6. The outermost planes ($i = 1$ and 7) have larger initial exposed surface areas and therefore initial slopes of the higher magnitude. On the other hand, all other planes have the same exposed (edge) surface and therefore identical initial slopes. The higher initial reaction rate of the outermost planes, however, creates additional exposed planar surfaces on the next set of planes ($i = 2$, 6), which then develop higher reactivity than their inner neighbors ($i = 3$, 5). These effects are mitigated with increase in A, due to lower initial reactivity, as shown in Figure 7, which depicts the results with $A = 3$ instead. In comparison to Figure 6 (for which $A = 2$) the initial slopes (and therefore reactivities) have lower magnitudes in Figure 7. Consequently, at any dimensionless time $\tau = k_2 t$ the expected number of remaining layers on any plane is larger for the case of $A = 3$.

Figures 8a–8c depict the expected evolution of the nonoverlapped crystallite for the parameter values used in Figure 6. Starting with the initial configuration in Figure 8a, with each plane having ten layers, the expected crystallite configuration at 20% conversion is shown in Figure 8b. The crystallite diameter is lowest at the outer planes and increases at the inner layers, creating exposed planar surfaces on the inner surfaces as well. These effects are even more pronounced at 50% conversion, as shown in Figure 8c. However, it is emphasized that these are only expected or mean configurations out of the large number (11^7) of possibilities. These possibilities include those configurations in which some internal planes have gasified more and have become smaller than the outer planes, including complete gasification of one or more internal planes. Examples of such configurations are provided in Figures 8d and 8e. These configurations create internal microporosity in the crystallites, such as that between the fourth and sixth planes from the bottom in Figures 8d and 8e, and between the first and fourth planes in Figure 8e. In Figure 8d the second plane from the bottom is completely reacted, and in the present approach it is assumed that the intracrystalline space so created is closed by the two planes coming together due to van der Waals interaction. This effect is assumed to lead to the homogeneous shrinkage observed by several recent workers. As a matter of interest at 50% conversion the probabilities of the configurations in Figures 8d and 8e were found to be 2.387×10^{-5} and 1.727×10^{-4}, respectively. Although these probabilities are low in comparison to unity, it is clear that they are significant given the large number of possibilities (11^7).

Conversion-time behavior

With time rendered dimensionless by scaling it with the reciprocal of the rate constant k_2 ($\tau = k_2 t$), the model has the five parameters A, H, m, e and ϵ_μ. The effect of each on the system behavior was therefore investigated. For the computations the parameters had the base values $H = 4$, $m = 8$, $\epsilon_{\mu 0} = 0.2$, $A = 2$, and $e = 3$, with one of these being varied at a time. Figures 9a–9e depict the effect of these parameters on the conversion-time behavior. In most of these cases sigmoidal curves are obtained, as is often found for reaction of carbons, suggesting a rate maximum during conversion. According to the model this is due to the initial increase in reactive area as the planar surfaces are exposed. Subsequently, however, as the crystallites become smaller, the total exposed area is reduced, leading to a decrease in rate with conversion. From the effect of varying the parameter A (see Figure 9a), it is evident that the model is sensitive to this surface chemistry parameter, leading to slowing down of the conversion with decrease in reactivity of the surface carbons, as reflected by the effect of increasing the value of A. The lower reactivity of the initial surface carbons is suggested to be due to the presence of attached functional groups, and can be controlled by surface treatment. Such treatment may be particularly useful for improving the stability of structural carbons as well as activated carbons to prolong their useful life. For chars produced in gasifiers and boilers, the surface chemistry is related to the parent coal properties and processing conditions and, to the author's knowledge, no other model captures the effect of this important variable.

From Figures 9b and 9c it is evident that larger crystallites (larger H or m) lower the rate, as is to be expected because of lowering of the specific surface area. Furthermore, for the case of $H = 1$ (that is, only one plane) sigmoidal behavior is not present, indicating a monotonic decrease in reaction rate.

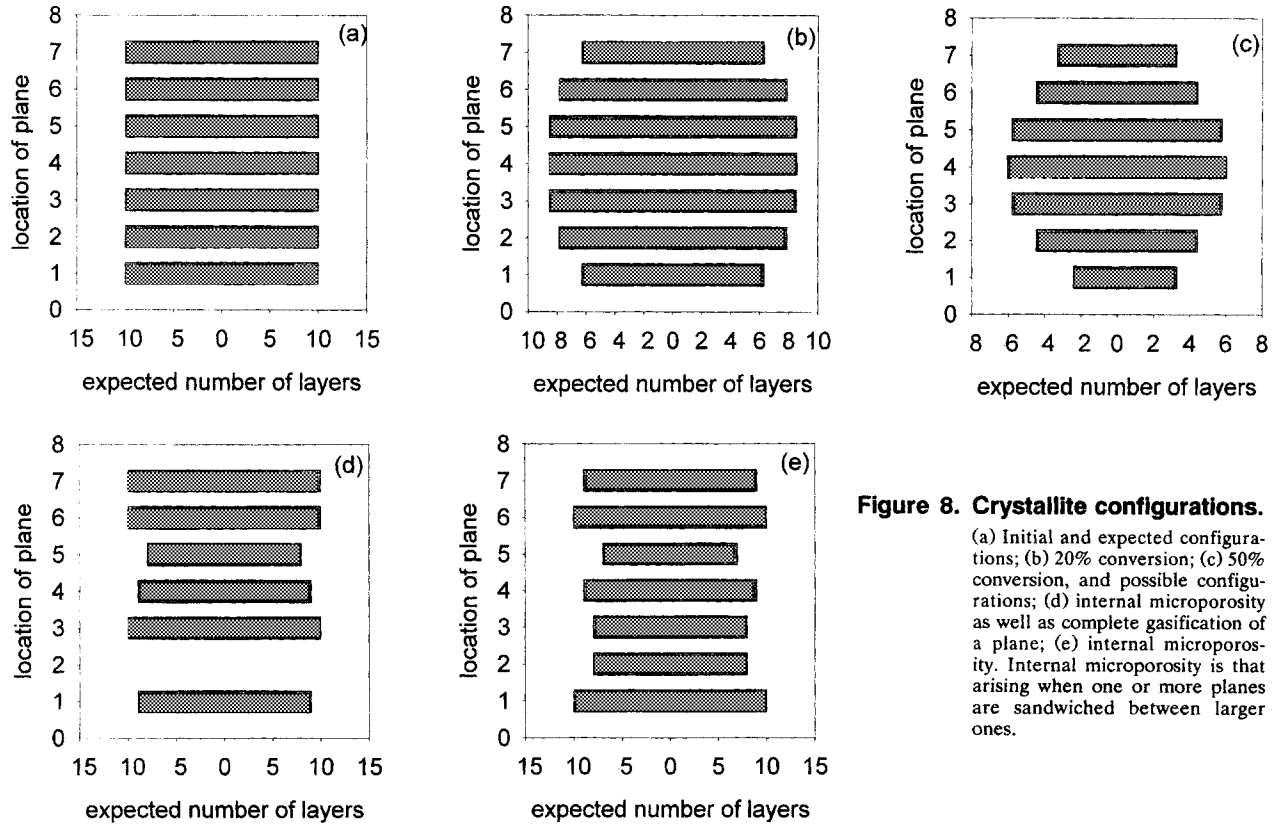

Figure 8. Crystallite configurations.

(a) Initial and expected configurations; (b) 20% conversion; (c) 50% conversion, and possible configurations; (d) internal microporosity as well as complete gasification of a plane; (e) internal microporosity. Internal microporosity is that arising when one or more planes are sandwiched between larger ones.

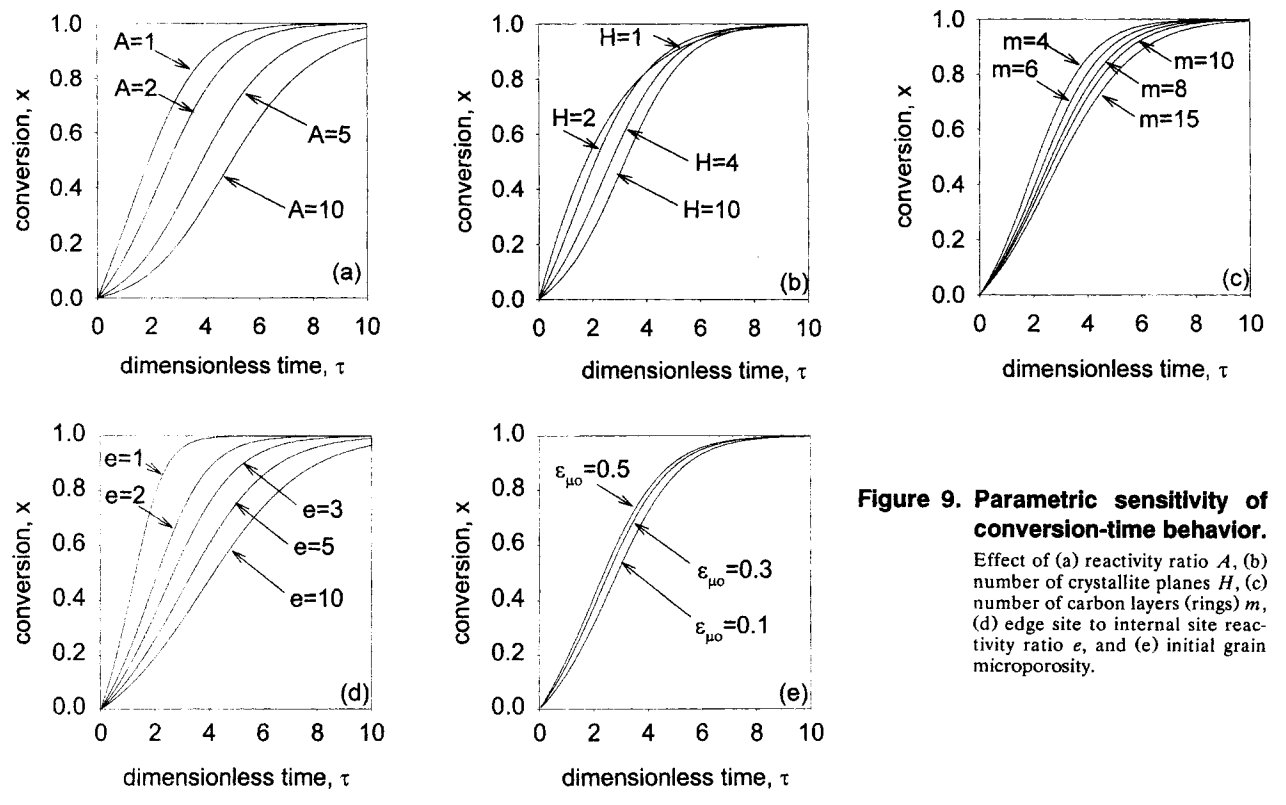

Figure 9. Parametric sensitivity of conversion-time behavior.

Effect of (a) reactivity ratio A, (b) number of crystallite planes H, (c) number of carbon layers (rings) m, (d) edge site to internal site reactivity ratio e, and (e) initial grain microporosity.

The effect of the parameter e is depicted in Figure 9d, showing it to have a strong influence on the reactivity. While the molecular orbital calculations of Kyotani et al. (1996) suggest that $e = 3$, as a reasonable average, it is to be expected that this value will vary with the type of surface site (D-type, armchair, or zig-zag) and location of the internal sites on the planes. Such complexity is not introduced here, but may be considered in future models involving more detailed representation of the aromatic structures on the planes. Certainly current analytical procedures need much further development to provide the necessary supporting data. Nevertheless, when this does become feasible, simulative techniques should be a desirable alternative to the prospect of introducing further complexity in the present model.

Figure 9e depicts the effect of the initial grain microporosity on the conversion-time behavior. At low values of the initial microporosity the reaction is slower due to the lower available nonoverlapped surface. Although the initial surface area is a maximum for $\epsilon_{\mu 0} = e^{-1}$ following Eq. 13, the effect of this parameter on the reactivity is more complex, as evident from Eqs. 34 and 37, leading to the behavior in Figure 9e.

Variation of reaction rate with conversion

Figures 10a–10e depict the effect of the different parameters on the variation of the calculated reaction rate with conversion, with base-case parameter values the same as for Figure 9. The results are consistent with those in Figure 9, confirming the rate maximum and sigmoidal behavior. For the case of $H = 1$ no rate maximum is observed, with the rate decreasing monotonically with conversion. In this case the surface area of the nonoverlapped crystallites must decrease with conversion, leading to the calculated reactivity behavior. Nevertheless, from the results in Figure 10 it may be anticipated that monotonically decreasing rate-conversion curves can also be obtained for other values of H for suitable values of the other parameters. In particular the strong effect of A on the location of the rate maximum may be noted in Figure 10a. With decrease in reactivity of the surface carbons (that is, increase in the value of A) not only was the rate lowered, but the position of the rate maximum shifted to higher conversion. This is due to the delayed opening up of the more reactive new sites on the planar edges. With increase in H as well as A, the rate maximum is shifted to higher conversions, because of increase in the number of internal planar surfaces that are gradually exposed and activated. The other parameters m, e, and $\epsilon_{\mu 0}$ affect the position of the rate maximum minimally, as seen in Figures 10c–10e, although both m and e have a strong effect on the magnitude of the rate. In all of these cases the rate maximum occurs in the vicinity of 40–50% conversion, and not significantly higher than the value of 39.33% predicted as the limiting position using the random pore model (Bhatia and Perlmutter, 1980). In that model this position was seen to be sensitive to an inherent structural parameter, a feature present also in the current model as evident from the sensitivity of the position to H. Nevertheless, the present model shows this position to be sensitive

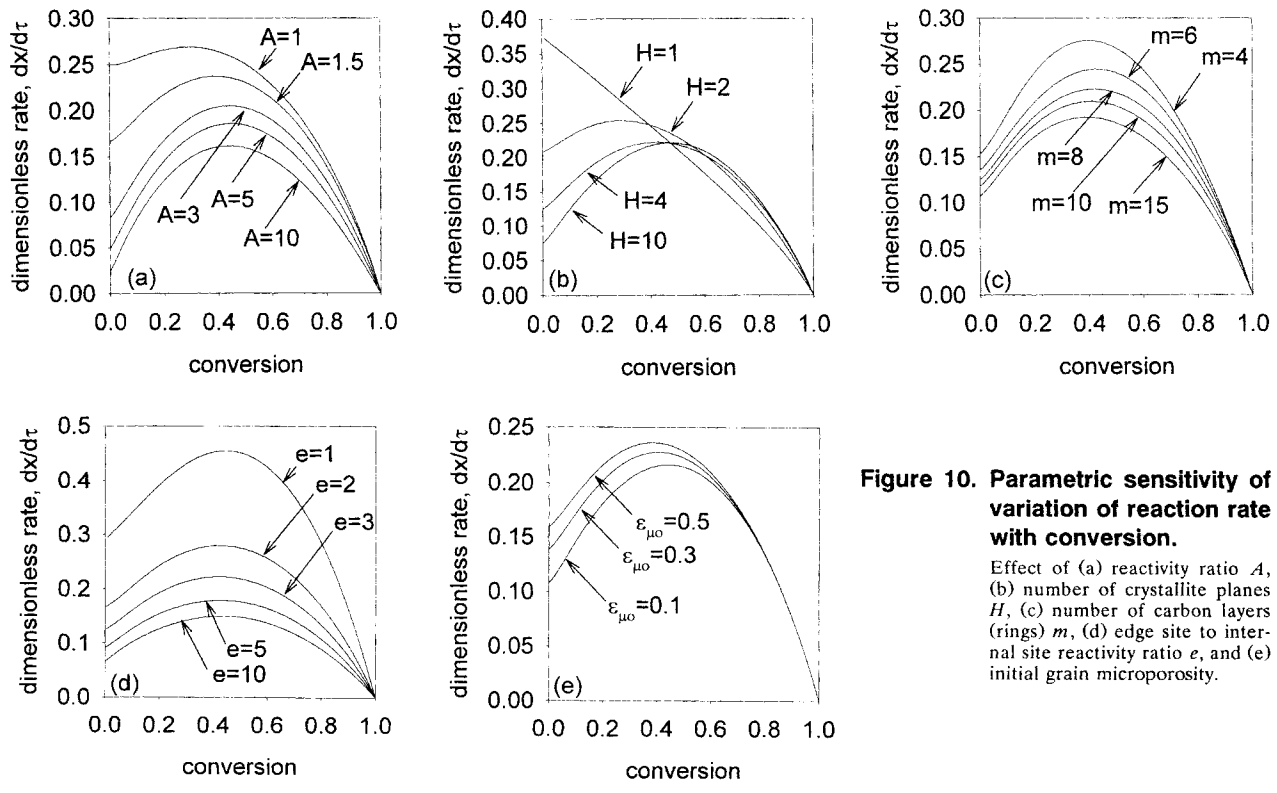

Figure 10. Parametric sensitivity of variation of reaction rate with conversion.

Effect of (a) reactivity ratio A, (b) number of crystallite planes H, (c) number of carbon layers (rings) m, (d) edge site to internal site reactivity ratio e, and (e) initial grain microporosity.

also to the kinetic parameter A, which is inversely related to the relative initial surface reactivity, a feature overlooked in prior models.

Particle shrinkage

Following the assumption of homogeneous shrinkage, as observed by Hurt et al. (1988), Eq. 28 permits the estimation of the relative particle volume at any time t. Figures 11a–11e depict the effect of the various parameters on the variation of relative particle volume with conversion, with base-case parameters the same as for Figure 9. The parameters A, m, and $\epsilon_{\mu 0}$ appear to have a very small effect on the relative particle volume, which decreases with conversion based on the proposed concept of shrinkage due to elimination of the intracrystalline space created when a plane is completely gasified. With increase in A (that is, decrease in relative surface reactivity) the shrinkage increases slightly since the probability of complete gasification of a plane, while others are partially reacted, increases. As seen in Figures 11b and 11c crystallites with a larger number of planes (larger H) shrink less, a feature in agreement with the observation of Walker (1995) that carbons having larger crystallites may be expected to shrink less. However, this is not entirely consistent with the predictions in Figure 11c, in which an increase in m initially leads to higher shrinkage. As seen in Figure 11d the relative edge reactivity is also very influential in determining the shrinkage, which reduces with increase in e (increase in the ratio of edge to normal reactivity of a plane). In most chars and carbons it may be anticipated that the crystallites have 3–7 planes (H lies between 3 and 7), and $e = 3$ based on the molecular orbital calculations of Kyotani et al. (1996). Since the other parameters have only a small influence, as seen in Figure 11, it may be expected that most chars and carbons will have similar variation of relative particle volume with conversion. This is indeed borne out by the literature data compiled by Hurt et al. (1993) in which similar curves are evident for an activated carbon, soot as well as a coal char. All these results also support the observation of Walker (1996) that interpretation of gasification data in the diffusion-affected regime must account for such shrinkage effects, as observed reductions in particle size cannot be entirely attributed to reaction at the external surface. In this connection it may be noted that if chemically controlled external reaction dominates then

$$\frac{R^3}{R_0^3} = 1 - x \tag{39}$$

which yields a straight line on the coordinates of Figure 11. The change in particle size due to shrinkage associated with internal conversion (Figure 11) is comparable to that predicted by Eq. 39, demonstrating the pitfalls and the need for careful data interpretation.

Although we have predicted the shrinkage based on the mechanism for eliminating the micropores created by complete gasification of planes, it may be noted that evidence exists (Wong et al., 1995) that some chars, notably those obtained at high temperatures (1,600°C), show little or no

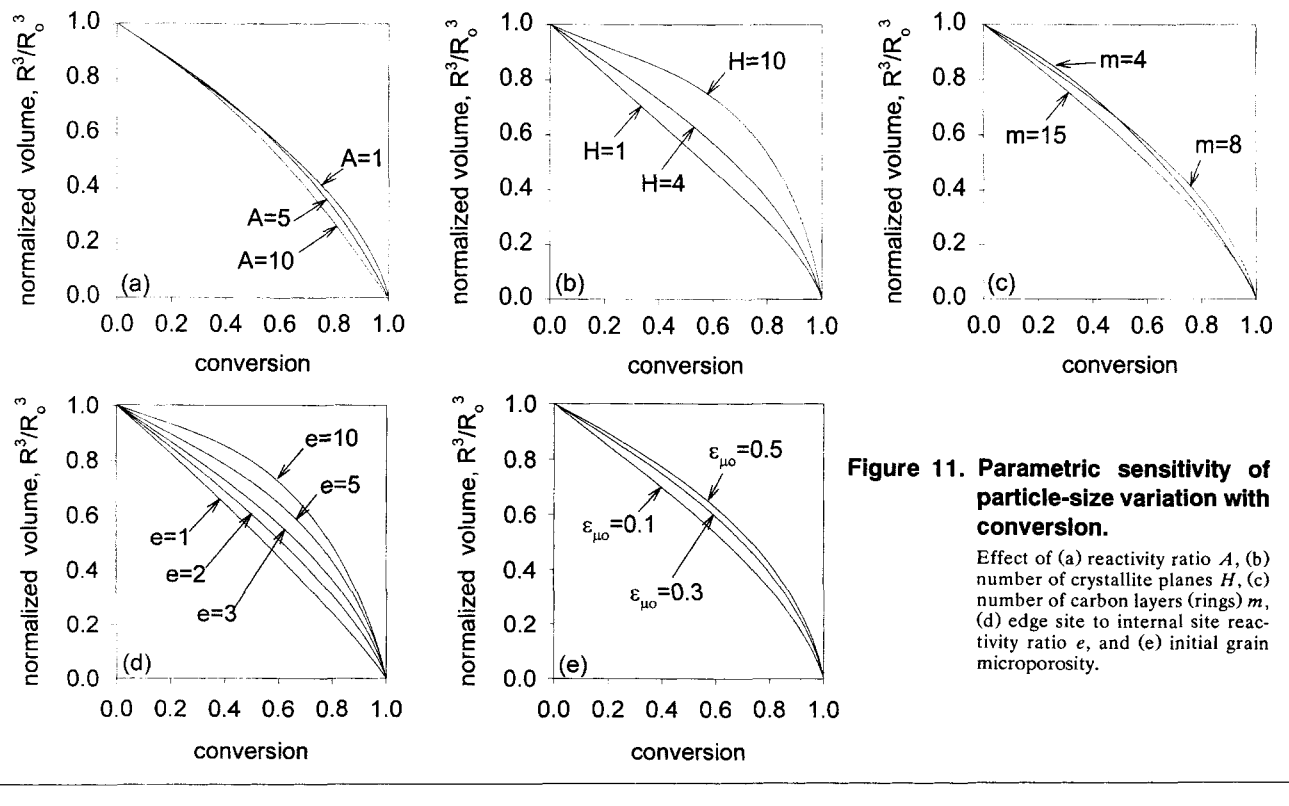

Figure 11. Parametric sensitivity of particle-size variation with conversion.

Effect of (a) reactivity ratio A, (b) number of crystallite planes H, (c) number of carbon layers (rings) m, (d) edge site to internal site reactivity ratio e, and (e) initial grain microporosity.

shrinkage. Based on the current results, such observations are consistent with the significantly lower surface areas and higher degrees of graphitization (higher values of H) expected of such chars. Furthermore, for the higher-temperature chars it may be anticipated that considerable annealing has occurred, leading to densification and decrease in flexibility of the solid, and therefore the observed absence of shrinkage. For such chars the current model needs modification, and this aspect will be investigated in our future work in the area. In the current context, where flexibility of the carbon skeleton is assumed, it may be noted that this feature has indeed been reported by Koresh (1993) who deduced this based on his unusual observation of adsorption hysteresis in the low pressure region.

Application to experimental data

To verify its applicability, the new model proposed here was applied to the data of Hurt et al. (1988) and d'Amore et al. (1991), who have reported the variation of reaction rate with conversion at various temperatures, for the low-temperature air-oxidation of Spherocarb (a commercially available activated carbon). While Hurt et al. have reported thermogravimetrically measured rates, d'Amore et al. have also reported rates measured in an electrodynamic balance. The absence of any significant particle size effects (based on experiments with particles of diameter 214 μm, and < 38 μm) as reported by Hurt et al. demonstrated reaction to be in the chemically controlled regime, with transport-related resistances being negligible. In addition, they have also provided data on variation of particle size with conversion of the Spherocarb, during reaction at temperatures of 495 and 600°C. In analyzing the rate data of Hurt et al. provided for these two temperatures, only the 600°C data was chosen, since the lower temperature data differed slightly from the more extensive data of d'Amore et al.

For the fitting of the rate data the parameter e was taken to have the value 3.0 following assumption (6). The values of the structural parameters H and m were estimated from published characterization data (Hurt et al., 1988; Waters et al., 1989) for Spherocarb. The data indicate that it has a total (BET) surface area of 864 m^2/g (Waters et al., 1988) or 665 m^2/cm^3 (Dudek, 1988), an external surface area of 5 m^2/g, and a mean micropore radius of 6.7 Å (Floess et al., 1988). These figures readily permit the estimation of S_g and $\epsilon_{\mu 0}$, which are found to have the values of 859 m^2/g and 0.39, respectively. Substituting these values into Eq. 13 enables selection of the set of integer values of m and H that provide a value of S_g as close as possible to 859 m^2/g. This method has been chosen here because more direct determinations of m and H by x-ray diffraction, as demonstrated by Babu and Seehra (1996), were not available for Spherocarb. Although many such sets of values for m and H may be obtained, typical x-ray characterization results (Babu and Seehra, 1996) suggest that in general H lies between 3 and 7, and m between 4 and 10, for most chars and nongraphitic carbons. With these restrictions, values of $H = 4$ and $m = 8$ could be readily identified as the most appropriate, providing $S_g = 857$ m^2/g. Thus, the model was applied to the Spherocarb reaction rate data of Hurt et al. (1988) at 600°C and of d'Amore et al. (1991) using the parameters $H = 4$, $m = 8$, $\epsilon_{\mu 0} = 0.39$, and $e = 3$, leaving only the parameters A and k_2 as unknowns.

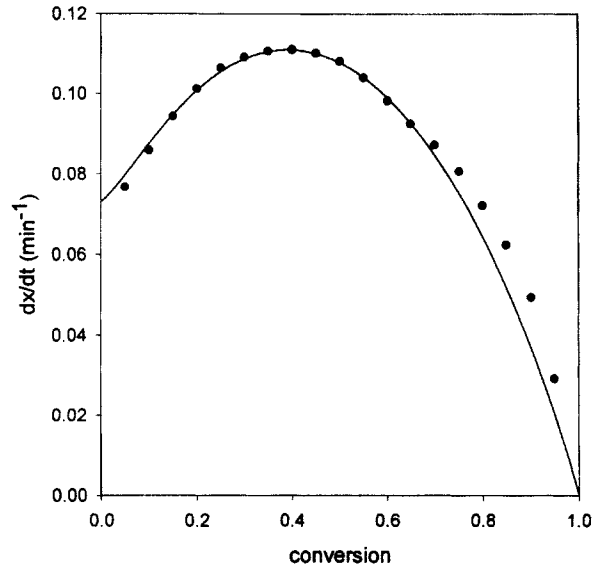

Figure 12. Variation of reaction rate with conversion for Spherocarb at 600°C.

Symbols represent data of Hurt et al. (1988), and the line represents current model calculations.

Figure 12 shows the agreement of the model to the data of Hurt et al., which provided $A = 1.93$ and $k_2 = 0.475$ min^{-1}. In estimating these values only the magnitude and location of the rate maximum was utilized, and not the rest of the experimental curve. For this estimation, A was first adjusted to obtain a match of the position of the rate maximum with the experimental value of $x = 0.4$, which yielded $A = 1.93$. This A value is unique since the position of the maximum is independent of the parameter k_2. k_2 was next adjusted so that the magnitude of the predicted maximum rate matched the experimental value, giving $k_2 = 0.475$ min^{-1}. Figure 12 shows that the agreement of the entire rate-conversion curve with the data is excellent despite the fact that only the coordinates of a single point (the rate maximum) have been fitted.

In addition to the above rate data Hurt et al. (1988) also provided their results for the variation of the particle size with conversion of the Spherocarb at various temperatures between 400°C and 600°C, given as the open circles and triangles in Figure 13. This particle size variation was reported by them to be entirely due to gasification-related shrinkage, since they concluded that negligible external surface reaction occurred, based on their observations that external surface features were retained. As discussed earlier, based on our model calculations, this shrinkage-related particle size variation is only minimally sensitive to the process parameters and may be considered nearly unique. The solid line in the figure provides the results of the present model, as predicted by Eq. 28, for the parameter values used for the Spherocarb, yielding excellent agreement with the data. This agreement is remarkable in view of the fact that the theoretical curve is completely predictive, based on the fit of the rate maximum in Figure 12, requiring no further fitting or parameter estimation. Also superimposed on the figure are the results of Ishi-

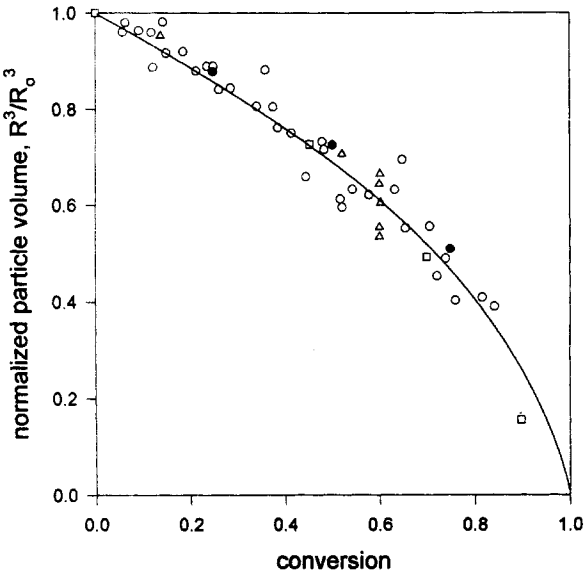

Figure 13. Variation of particle size with conversion.

Symbols represent data from various sources as described in the text, and the line represents current model predictions.

guro et al. (1991), represented by filled circles in Figure 12, and of Kandas (1997), given by open squares, for the shrinkage of soot. The soot data are also generally consistent with the Spherocarb data and our theoretical curve, further supporting the new model and our assertion that the gasification-induced particle-size variation with conversion is only weakly process parameter and char/carbon dependent for most nongraphitic carbons with H of around 3–7.

In addition to the data analyzed above d'Amore et al. (1991) reported rate-conversion results for air-oxidation of spherocarb at various temperatures in a thermogravimetric analyzer as well as an electrodynamic balance. To analyze the data it was assumed that the parameter A is temperature-independent, so that the rate expression

$$\frac{dx}{dt} = k_2 g(x, A, e) \tag{40}$$

can be rewritten in dimensionless form as

$$\frac{dx}{d\tau^*} = f(0.5, A, e) g(x, A, e) \tag{41}$$

where $\tau^* = t/t_{1/2} = \tau/\tau_{1/2}$, and

$$\tau_{1/2} = k_2 t_{1/2} = f(0.5, A, e) = \int_0^{0.5} \frac{dx}{g(x, A, e)} \tag{42}$$

For temperature-independent values of A (= 1.93, based on the above fit of the 600°C data of Hurt et al.) and $e = 3$, Eq. 41 provides a convenient scaling for the effect of temperature on rate. Based on the 600°C fit discussed above the value of $f(0.5, A, e)$ was estimated from our model as 2.416. Figure 14 depicts the comparison of the theoretical predictions and experimental data of d'Amore et al. (1991), when plotted in accordance with Eq. 41. The larger scatter of the data from the electrodynamic balance is clearly evident. Nevertheless, the results do not demonstrate any consistent trend with temperature, supporting the assumption of temperature independence of A and e. The good agreement between model predictions and the data, without the use of any fitting parameters, also further supports the new approach.

Summary and Conclusions

A new probabilistic model for the reaction of chars and carbons has been developed here that considers the chemistry and turbostratic structure of the graphitic planes, which represent a significant component of the true structure. The model considers the well-known anisotropic reactivity of the carbon crystallites by incorporating different rate constants for the propagation of reaction perpendicular to the edges of the faces of the graphene planes, with a ratio of $e = 3$ being suggested by molecular orbital calculations.

Furthermore, the influence of the functional groups on the initial crystallite surfaces is considered by incorporating a different rate constant for the initial surface sites. With this mechanism the possibility of random complete gasification of a crystallite plane before its neighbors is enhanced if the initial edge carbons have lower reactivity, as is to be expected by the presence of the functional groups. This mechanism may be responsible for the shrinkage in the chemically controlled regime. The model has been found to correctly predict this phenomenon and match experimental data on particle size variation with conversion, with fitting parameters determined entirely from rate data.

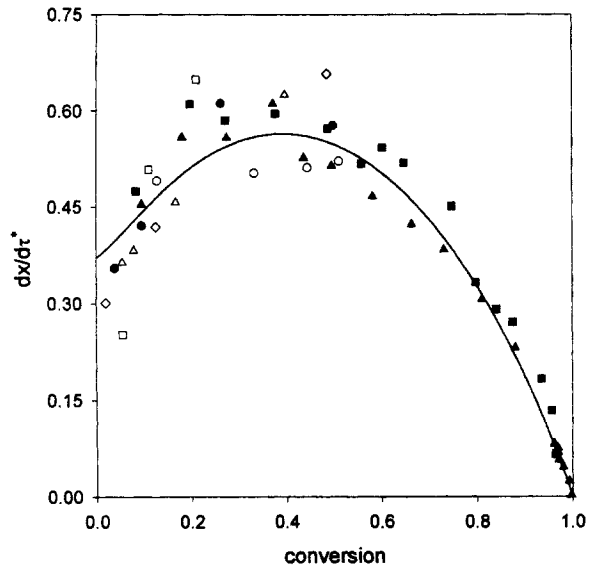

Figure 14. Variation of reaction rate with conversion for Spherocarb at various temperatures.

From D'Amore et al. (1991). Filled symbols represent data measured in a thermogravimetric analyzer: ● = 673 K, ■ = 693 K, ▲ = 768 K. Open symbols represent data obtained in an electrodynamic chamber: □ = 764 K, ○ = 820 K, ◇ = 948 K, △ = 1,033 K. The line represents current model predictions.

Based on the model-computations results, it is evident that the surface chemistry is important in determining reaction rates and particle shrinkage. This feature was overlooked in prior models, which also did not incorporate any mechanism for particle shrinkage. With decrease in initial surface reactivity, not only is the reaction slower but the shrinkage is larger. The shrinkage will be of much concern in the diffusional regime where particle size plays an important role. Consequently, further detailed investigations of the shrinkage and more direct confirmation of the proposed mechanism are recommended.

The model proposed here lumps the effect of surface chemistry into the single rate constant k_1. Clearly this is a first approximation that may be improved on in the future with more detailed representation of the surface groups and associated rate constants. This complexity will obviously require detailed characterization and observation of reaction of these groups progressively with conversion. Alternatively this can be considered as a surface heterogeneity, as is common in analysis of adsorption data, manifested through a distribution of the rate constant k_1. This can be conveniently investigated with the proposed model and will be reported later.

The number of planes in a crystallite is another important variable that strongly affects the rate and shrinkage. For larger crystallites (larger number of planes as well as larger diameter) the rate is reduced, as would be expected. However, the shrinkage is most sensitive to the number of crystallite planes. An increase in the number of crystallite planes reduces shrinkage. Graphitization is expected to reduce shrinkage because the number of planes increases. Thus, higher temperature chars may shrink much less due to larger values of H. Although this feature needs to be confirmed through more extensive data, the importance of detailed characterization at the crystallite level is clear.

Acknowledgments

The author wishes to acknowledge the financial support provided by the Cooperative Research Centre for Black Coal Utilization, which is funded in part by the Cooperative Research Centres Program of the Commonwealth Government of Australia. The author also acknowledges the financial support of the Australian Research Council.

Notation

f = fractional loss in volume of solid phase
$g(x, A, e)$ = functional dependence of rate on conversion, A and e
$k_{in}^{(1)}$ = rate constant of internal planar sites for plane i when it has edge location n, and is attacked on its upper exposed surface
$k_{in}^{(2)}$ = rate constant of internal planar sites for plane i when it has edge location n, and is attacked on its lower exposed surface
M_c = atomic weight of carbon
N_a = Avogadro number
N_{Li} = expected number of layers in ith plane
N_t = total number of carbon atoms in a plane
N_v^0 = initial value of N_v
q_i = probability that ith plane is completely reacted
Q = fractional shrinkage
R = particle radius
$R_{ink}^{(j)}$ = jth contribution to R_{ink}, defined in Eqs. 21–24
S_{eg} = initial specific area of nonoverlapped crystallites
S_g = initial specific surface area
$t_{1/2}$ = time to reach 50% conversion
V_c = volume of a crystallite

Greek letters

$\epsilon_{\mu 0}$ = initial value of grain microporosity
ρ_t = crystallite density

Literature Cited

Adschiri, T., T. Kojima, and T. Furasawa, "Estimation of Dynamic Change in Gasification Rate of Chars—II. Overlapped Grain Model," *Chem. Eng. Sci.*, **42**, 1319 (1987).
Babu, V. S., and M. S. Seehra, "Modelling of Disorder and X-Ray Diffraction in Coal-Based Graphitic Carbons," *Carbon*, **34**, 1259 (1996).
Ben-Aim, R. I., "Influence of Structural Parameters on the Mechanism of Combustion of Coal," *Int. Chem. Eng.*, **27**, 70 (1987).
Bhatia, S. K., "On the Apparently Quasi-Steady Catalytic Surface," *Chem. Eng. Sci.*, **42**, 2972 (1987a).
Bhatia, S. K., "Modeling the Pore Structure of Coal," *AIChE J.*, **33**, 1707 (1987b).
Bhatia, S. K., "Perturbation Analysis of Gas Solid Reactions: I. Solid of Low Initial Permeability," *Chem. Eng. Sci.*, **46**, 173 (1991a).
Bhatia, S. K., "Perturbation Analysis of Gas Solid Reactions: II. Reduction to the Diffusion-Controlled Shrinking Core," *Chem. Eng. Sci.*, **46**, 1465 (1991b).
Bhatia, S. K., and J. S. Gupta, "Mathematical Modelling of Gas-Solid Reactions: Effect of Pore Structure," *Rev. Chem. Eng.*, **8**, 177 (1992).
Bhatia, S. K., and D. D. Perlmutter, "A Random Pore Model for Fluid Solid Reactions: I. Isothermal Kinetic Control," *AIChE J.*, **26**, 379 (1980).
Bhatia, S. K., and B. J. Vartak, "Reaction of Microporous Solids," *Carbon*, **34**, 1383 (1996).
Biscoe, J., and B. E. Warren, "X-Ray Study of Carbon Black," *J. Apply. Phys.*, **13**, 364 (1942).
Bonnetain, L., and G. Hoynant, *Les Carbones*, Masson, Paris, p. 277 (1965).
Chen, S. G., R. T. Yang, F. Kapteijn, and J. A. Moulijn, "A New Surface Oxygen Complex on Carbon: Toward a Unified Mechanism for Carbon Gasification Reactions," *Ind. Eng. Chem. Res.*, **32**, 2835 (1993).
Chi, W. K., and D. D. Perlmutter, "The Effect of Pore Structure on the Char Steam Reaction," *AIChE J.*, **35**, 1791 (1989).
D'Amore, M., L. Tognotti, and A. F. Sarofim, "Morphological Changes during Oxidation of a Single Char Particle," *Fuel Chemistry*, Amer. Chem. Soc., p. 939 (1991).
Davis, K. A., R. H. Hurt, N. Y. C. Yang, and T. Headley, "Evolution of Char Chemistry, Crystallinity, and Ultrafine Structure during Pulverized-Coal Combustion," *Proc. Int. Symp. on Comb.*, Los Angeles (1994).
Dudek, D. R., PhD Thesis, MIT, Cambridge, MA (1988).
Easler, T. E., R. C. Bradt, and P. L. Walker, "Gasification-Induced Densification of Form Coke," *Fuel*, **69**, 124 (1990).
Franklin, R. E., "Crystallite Growth in Graphitizing and Non-Graphitizing Carbons," *Proc. Roy. Soc. London Ser. A.*, **209**, 196 (1951).
Gavalas, G. R., "A Random Capillary Model with Application to Char Gasification at Chemically Controlled Rates," *AIChE J.*, **26**, 577 (1980).
Hennig, G. R., "Anisotropic Reactivities of Graphite. I. Reactions of O_2 and Graphite," *Carbon*, **3**, 107 (1965).
Horton, W. S., "Oxidation Kinetics of Pyrolytic Graphite," *Proc. of the 5th Conf. on Carbon*, Pergamon Press, Oxford, p. 233 (1961).
Hurt, R. H., D. R. Dudek, J. P. Longwell, and A. F. Sarofim, "The Phenomenon of Gasification-Induced Carbon Densification and Its Influence on Pore Structure Evolution," *Carbon*, **26**, 433 (1988).
Hurt, R. H., A. F. Sarofim, and J. P. Longwell, "Gasification-Induced Densification of Carbons: From Soot to Form Coke," *Comb. Flame*, **95**, 430 (1993).
Ishiguro, T., N. Suzuki, Y. Fujitani, and H. Morimoto, "Microstructural Change of Diesel Soot During Oxidation," *Comb. Flame*, **85**, 1 (1991).

Kandas, A. W., PhD Thesis, MIT, Cambridge (1997).
Kantorovich, I. I., and E. Bar-Ziv, "Processes in Highly Porous Chars under Kinetically Controlled Conditions: I. Evolution of the Porous Structure," *Comb. Flame*, **97**, 61 (1994).
Kasaoka, S., Y. Sakata, and C. Tong, "Kinetic Evaluation of the Reactivity of Various Coal Chars for Gasification with Carbon Dioxide in Comparison with Steam," *Int. Chem. Eng.*, **25**, 160 (1985).
Koresh, J. E., "On the Flexibility of the Carbon Skeleton," *J. Chem. Soc. Farad. Trans.*, **89**, 935 (1993).
Kyotani, T., K. C. Ito, A. Tomita, and L. R. Radovic, "Monte Carlo Simulation of Carbon Gasification using Molecular Orbital Theory," *AIChE J.*, **42**, 2303 (1996).
Kyotani, T., C. A. Lyon y Leon, and L. R. Radovic, "Simulation of Carbon Gasification using an Edge Recession Model," *AIChE J.*, **39**, 1178 (1993).
Laine, N. R., F. J. Vastola, and P. L. Walker, "Role of the Surface Complex in the C-O Reaction," *Proc. Conf. on Carbon*, Pergamon Press, p. 211 (1961).
Letort, M., "Le Mécanisme Fondamental de Combustion du Carbone," *Rev. Univ. des Mines*, **16**, 255 (1960).
Lizzio, A. A., H. Jiang, and L. R. Radovic, "On the Kinetics of Carbon (Char) Gasification: Reconciling Models with Experiments," *Carbon*, **28**, 7 (1990).
Menendez, J. A., J. Phillips, B. Xia, and L. R. Radovic, "On the Modification and Characterization of Chemical Surface Properties of Activated Carbon—In the Search of Carbons with Stable Basic Properties," *Langmuir*, **12**, 4404 (1996).
Miura, K., and K. Hashimoto, "A Model Representing the Change of Pore Structure During the Activation of Carbonaceous Materials," *Ind. Eng. Chem. Proc. Des. Dev.*, **23**, 138 (1984).
Miura, K., M. Makino, and P. L. Silveston, "Correlation of Gasification Reactivities with Char Properties and Pyrolysis Conditions using Low Rank Canadian Coals," *Fuel*, **69**, 580 (1990).
Moulijn, J. A., and F. Kapteijn, "Towards a Unified Theory of Reactions of Carbon with Oxygen-Containing Molecules," *Carbon*, **33**, 1155 (1995).
Petersen, E. E., "Reaction of Porous Solids," *AIChE J.*, **3**, 442 (1957).
Rudzinski, W., and D. H. Everett, *Adsorption of Gases on Heterogeneous Surfaces*, Academic Press, London (1992).
Seaton, N. A., J. P. R. B. Walton, and N. Quirke, "A New Analysis Method for the Determination of the Pore Size Distribution of Porous Carbons from Nitrogen Adsorption Measurements," *Carbon*, **27**, 853 (1989).
Senneca, O., P. Russo, P. Salatino, and S. Masi, "The Relevance of Thermal Annealing to the Evolution of Char Gasification Reactivity," *Carbon*, **35**, 141 (1997).
Su, J. L., and D. D. Perlmutter, "Effect of Pore Structure on Char Oxidation Kinetics," *AIChE J.*, **31**, 973 (1985).
Szekely, J., J. W. Evans, and H. Y. Sohn, *Gas-Solid Reactions*, Academic Press, New York (1976).
Thomas, J. M., and K. M. Jones, "Kinetic Anisotropy in the Oxidation of Graphite," *J. Nucl. Mater.*, **11**, 236 (1964).
Walker, P. L., "Complications Introduced from Gasification-Induced Densification of Disordered Carbons," *Carbon*, **34**, 1603 (1996).
Waters, B. J., R. G. Squires, N. M. Laurendreau, and R. E. Mitchell, "Evidence for the Formation of CO_2 in the Vicinity of Burning Pulverized Carbon Particles," *Comb. Flame*, **74**, 91 (1988).
Wolff, W. F., "A Model of Active Carbons," *J. Phys. Chem.*, **63**, 653 (1959).
Wong, B. A., G. R. Gavalas, and R. C. Flagan, "Effect of Char Formation Temperature on the Densification of Bituminous Coal Char During Gasification," *Energy and Fuels*, **9**, 493 (1995).
Yang, R. T., and R. Z. Duan, "Kinetics and Mechanism of Gas-Carbon Reations: Confirmation of Etch Pits, Hydrogen Inhibition and Anistropy in Reactivity," *Carbon*, **23**, 325 (1985).

Manuscript received May 8, 1998, and revision received Aug. 10, 1998.